Dynamics of vacancies in two-dimensional Lennard-Jones crystals

Zhenwei Yao[1] and Monica Olvera de la Cruz[1,2,3,4]

[1]*Department of Materials Science and Engineering, Northwestern University, Evanston, Illinois 60208-3108, USA*
[2]*Department of Chemistry, Northwestern University, Evanston, Illinois 60208-3108, USA*
[3]*Department of Chemical and Biological Engineering, Northwestern University, Evanston, Illinois 60208-3108, USA*
[4]*Department of Physics, Northwestern University, Evanston, Illinois 60208-3108, USA*

Vacancies represent an important class of crystallographic defects, and their behaviors can be strongly coupled with relevant material properties. In this work, we study the dynamics of generic n-point vacancies in two-dimensional Lennard-Jones crystals in several thermodynamic states. Simulations reveal the spectrum of distinct, size-dependent vacancy dynamics, including the nonmonotonously varying diffusive mobilities of one-, two- and three-point vacancies, and several healing routines of linear vacancies. Specifically, we numerically observe significantly faster diffusion of the two-point vacancy that can be attributed to its rotational degree of freedom. The high mobility of the two-point vacancies opens the possibility of doping two-point vacancies into atomic materials to enhance atomic migration. The rich physics of vacancies revealed in this study may have implications in the engineering of defects in extensive crystalline materials for desired properties.

I. INTRODUCTION

Defects naturally occur in almost all crystalline materials [1–4]. Specific defects are artificially introduced in a variety of industrial materials like silicon crystals, graphenes, and metals to achieve desired properties [5,6]. Vacancy defects have received increasing attention in the past decades for their crucial role in the migration of atoms [7], the melting and growth of crystals [8–10], the crystallization of DNA-programmable nanoparticles [11], and even as promising candidates for achieving quantum tunneling in quantum solids [12]. Understanding the physics of vacancies would lay the foundation for the engineering of new materials at multiple length scales [5,13,14]. However, it is a challenge to directly track vacancies in three-dimensional atomic materials [13]. To address this problem, mesoscopic two-dimensional colloidal crystals serve as an excellent model system for studying crystallographic defects [13,15–19]. The spontaneous formation of two-dimensional colloidal crystals has been directly observed in experiments using either the pure repulsive electrostatic interaction [13,15,16] or the balance of the electrohydrodynamic attraction and the electrostatic repulsion [17]. An n-point vacancy with n missing particles was created by dragging away n particles with optical tweezers [13,15,16].

Previous studies mostly focused on the dynamics of small vacancies with $n \leqslant 3$ at a fixed temperature [13,15–17,20]. The problem of how the vacancy dynamics depends on vacancy size and temperature is still unclear. In addition, it appears that the behavior of vacancies is very sensitive to the nature of the interaction potential through a survey of the energetics [21–24] and dynamics [25–29] of vacancies in two-dimensional crystals with the Yukawa potential [25,27–29], Gaussian core [30], the repulsive $1/r^3$ potential [23], the purely repulsive Weeks-Chandler-Andersen potential [20], and the Lennard-Jones potential [21,22]. The generic, formally simple Lennard-Jones (L-J) potential represents an important form of interaction that has been extensively used to model a large variety of chemical and physical bonds [31]. The revealed vacancy physics in the

L-J system is therefore applicable to understanding a host of vacancy-mediated phenomena in crystalline materials like crack initiation, the stress-strain relation, and other associated structural properties of crystals [32]. The examination of the energetics of vacancies in L-J crystals suggested that a sufficiently deep valley in the curve of the interaction potential is essential to support intact vacancies [21,22]. In contrast, the integrity of vacancies was hardly observed in systems of purely repulsive particles where the n-point vacancies tend to collapse into various defect clusters [15,28,33–35]. We therefore expect a distinct scenario of vacancy dynamics in L-J crystals.

In this work, we perform MD simulations to systematically study the dynamics of generic n-point vacancies in two-dimensional L-J crystals at several thermodynamic states. We will focus on the NPT ensemble with zero external pressure, while the NAT ensemble will be employed to study the dependence of the vacancy mobility on the particle density. The integrity of the one-point vacancy is found to be well preserved even in its thermally excited hoppings over the crystal; the super stability of one-point vacancies is discussed in terms of the underlying topological defect structures. We numerically observe that the two-point vacancy has a much higher mobility than the one-point vacancy despite of its larger size, while the mobility of the three-point vacancy is significantly reduced. These intriguing phenomena are discussed in terms of the increased number of vacancy configurations in the two- and three-point vacancies. The significantly faster diffusion of the two-point vacancy in comparison with the one- and three-point vacancies opens the possibility of doping two-point vacancies into atomic materials to enhance the efficiency of atoms migration. Simulations also capture the details of the spontaneous zipping of an initially open, linear vacancy to form a belt with square lattice ordering in the hexagonal crystal. Depending on the vacancy length, this geometrically incompatible beltlike object conforms to distinct dynamic modes, including the breathing mode, and the collective modes of uniform translation and rotation. We finally report that the increasing particle density in L-J crystals tends to immobilize vacancies. The revealed rich physics

of vacancies as well as their connection with topological defects may have implications in the engineering of defects in extensive crystalline materials.

II. METHOD

We employ the molecular dynamics simulator LAMMPS [36] to study the vacancy dynamics in two-dimensional L-J crystals [37]. We first construct a rectangular two-dimensional hexagonal lattice of N particles with the periodic boundary condition to mimic an infinitely large crystal. $N = 20\,000$ unless otherwise specified. The lattice spacing is the balance distance $r_m = 2^{1/6}\sigma_0 \approx 1.1225\sigma_0$ of the adopted L-J potential $V(r) = 4\epsilon_0[(\sigma_0/r)^{12} - (\sigma_0/r)^6]$, with a cutoff length $r_{\text{cut-off}} = 2.5\sigma_0$. Throughout this work, the energy (as well as the temperature for the Boltzmann constant $k_B = 1$) and the length are measured in the units of σ_0 and ϵ_0, respectively. The unit of time is $\tau_0 = \sigma_0(m/\epsilon_0)^{1/2}$, where m is the mass of the particle. An n-point vacancy is created by deleting n particles at desired lattice sites. The initial temperature of the system is specified by a Gaussian distribution of velocity over all particles. The motion of particles is confined in the plane. The trajectory of motion is obtained by performing time integration on Nose-Hoover-style non-Hamiltonian equations of motion which can generate positions and velocities sampled from the isothermal-isobaric ensemble [37]. The configuration of particles is updated for every time step $\Delta t = 0.005\tau_0$. We compile C++ codes to perform data analysis, including the Delaunay triangulation [9] and the identification and tracking of the vacant sites. To exclude the possible finite size effect, we also simulate the diffusion of one-point particle at $T = 0.25$ in the systems of $N = 7199$ and $N = 12\,799$, and compare the numerically measured diffusion coefficients with the value in the original system of $N = 19\,999$. We find that the finite size effect can be eliminated at least for $N > 12\,799$.

III. RESULTS AND DISCUSSION

We first study the behaviors of the one-point vacancy. Simulations show that below the melting temperature the integrity of the one-point vacancy is well preserved even in
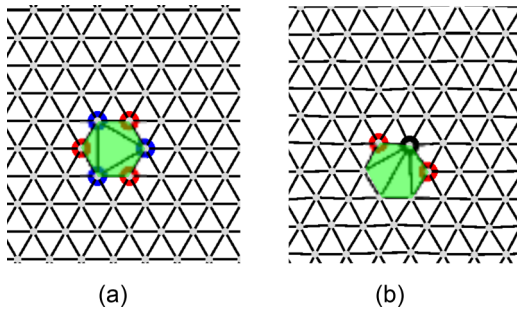

FIG. 1. (Color online) The topological defect structure associated with the one-point vacancy in a perfect hexagonal lattice (a) and at finite temperature (b). The red, blue, and black dots represent five-, seven-, and eight-fold disclinations, respectively. A slight fluctuation of the particles gives rise to distinct defect motifs. The region of the vacancy is shadowed in green.
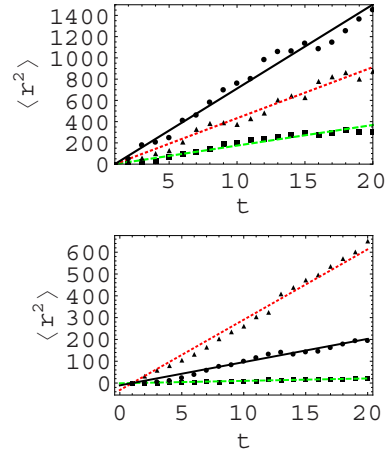

FIG. 2. (Color online) The mean squared displacement $\langle r^2 \rangle$ vs time over 20 independent runs in MD simulations. (a) The case of one-point vacancy. From above to below, $T = 0.3, 0.28$, and 0.25, respectively. The slopes are $79.05, 48.03$, and 19.40 (in the unit of $\sigma_0^2/2500\tau_0$). (b) From above to below lists the cases of two-point (triangles, dotted, red), three-point (dots, solid, black), and one-point (squares, dashed, green) vacancies, whose slopes are $32.28, 10.66$, and 1.11 (in the unit of $\sigma_0^2/2500\tau_0$), respectively. $T = 0.2$. The unit of time is $2500\tau_0$.

its hopping over the crystal lattice. The sixfold symmetry of the intact one-point vacancy is compatible with the crystal where it lives. To understand the super stability of the one-point vacancy supported by the L-J potential, we examine its topological defect structure which is revealed by the Delaunay triangulation [9]. The elementary topological defects in two-dimensional hexagonal lattices are disclinations which are vertices surrounded by p nearest neighbors with $p \neq 6$. The disclinations associated with the one-point vacancy in a perfect hexagonal crystal constitute a necklace of alternating five- and seven-fold disclinations [see Fig. 1(a)]. This defect motif transforms with the positional fluctuation of the particles around the vacant site, as shown in Fig. 1(b). Despite the thermally driven transfer of topological charges among the disclinations, the net topological charge around the vacancies is always zero conforming to the topological requirement [9].
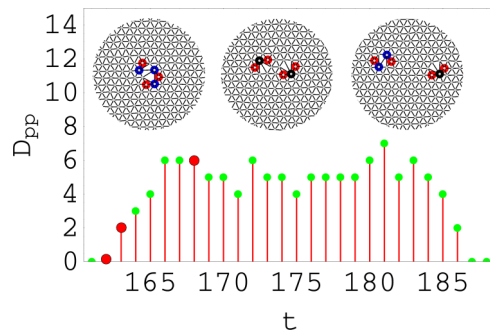

FIG. 3. (Color online) The distance D_{pp} between two one-point vacancies vs time at $T = 0.25$. The three configurations in the insets are at $t = 162, 163$, and 168, in the unit of $25\tau_0$. The red, blue, and black dots represent five-, seven-, and eight-fold disclinations, respectively.
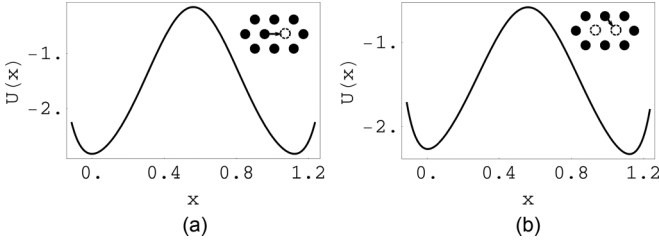
FIG. 4. The energy variation when a neighboring particle moves to fill a vacant site for the case of one-point vacancy (a) and two-point vacancy (b). The height of the energy barrier is read as 2.69 (a) and 1.68 (b). The lattice spacing is $a = r_m$. The energy and length are measured in the unit of ϵ_0 and σ_0.

Energetically, these topologically neutral, tightly bound defect "multipoles" impose negligible influence on the stress distribution in the crystal [9,38]. Note that such a bound structure of defects stably existing in planar geometries can be pulled apart on a sufficiently curved surface with spatially varying curvature [39,40]. The energetically favored inseparability of the associated defect clusters in planar crystals, however, does not exclude the possibility of their translational motion as a whole along one of the six symmetric axes of the hexagonal crystal.

At finite temperature, the one-point vacancy has some probability to jump to a neighboring lattice point; this thermally excited process is realized by a neighboring particle moving in to fill the vacant site. In the energy landscape for the one-point vacancy over the crystal lattice, every lattice point corresponds to the bottom of the energy valley. An energy barrier must be conquered by the one-point vacancy to escape from the valley. The shape of the energy landscape resembles that of a hexagonal egg crate. The energy of the system is degenerate when the one-point vacancy jumps from one valley to another. The one-point vacancy is numerically observed to drift away from the origin point. We track the mean squared displacement $\langle r^2 \rangle$ over a number of independent runs

at different temperatures. Simulations show that the $\langle r^2 \rangle - t$ curve converges to a straight line with the increase of the number of simulation runs; it is the signature of diffusion as well as an indicator of reliable simulations [see Fig. 2(a)]. We therefore confirm the diffusive nature of the one-point vacancy.

To explore the nature of the diffusive motion of a point vacancy in the crystal, we propose a random walk model on a two-dimensional hexagonal lattice. Consider a walker initially at $z = 0$ on a complex plane. In the time interval δt, it has the identical probability p_m to jump to one of the six nearest neighbors, and the probability p_0 to stay in the original site. $6p_m + p_0 = 1$. The position of the walker after N steps is

$$z_N = \sum_{j=1}^{N} r_j \exp(i\theta_j). \tag{1}$$

For an arbitrary step j, either $r_j = 0$ (the walker does not move) or $r_j = \ell$ and θ_j takes one value from $\{0, \pi/3, \ldots, 5\pi/3\}$ with the same probability. It is straightforward to check that $\langle z_N \rangle = 0$ as expected. At step j, $\langle r_j^2 \rangle = \ell^2 \times (1 - p_0) + 0 \times p_0 = \ell^2(1 - p_0)$. We assume the statistical independence between consecutive steps, i.e., $\langle r_j r_k \exp(i\theta_j - \theta_k) \rangle$ can be written as the product of $\langle r_j \exp(i\theta_j) \rangle$ and $\langle r_k \exp(i\theta_k) \rangle$, both of which are zero. By making use of these equalities, We finally obtain the mean squared displacement

$$\langle |z_N|^2 \rangle = (1 - p_0)N\ell^2 = 2D't, \tag{2}$$

where $D' = (1 - p_0)D$ and $D = \ell^2/(2\delta t)$. In the parameter p_0 contains the microscopic information about the depth of the potential well. Equation (2) shows that the stay in the original site ($p_0 \neq 0$) does not change the diffusive nature of the dynamics of the particle; a nonvanishing p_0 only reduces the particle mobility. The derived mean squared displacement Eq. (2) also applies for random walk on square lattice and off-lattice. The diffusive nature of the dynamics of the one-point vacancy is therefore well captured by the random walk model on the hexagonal lattice.
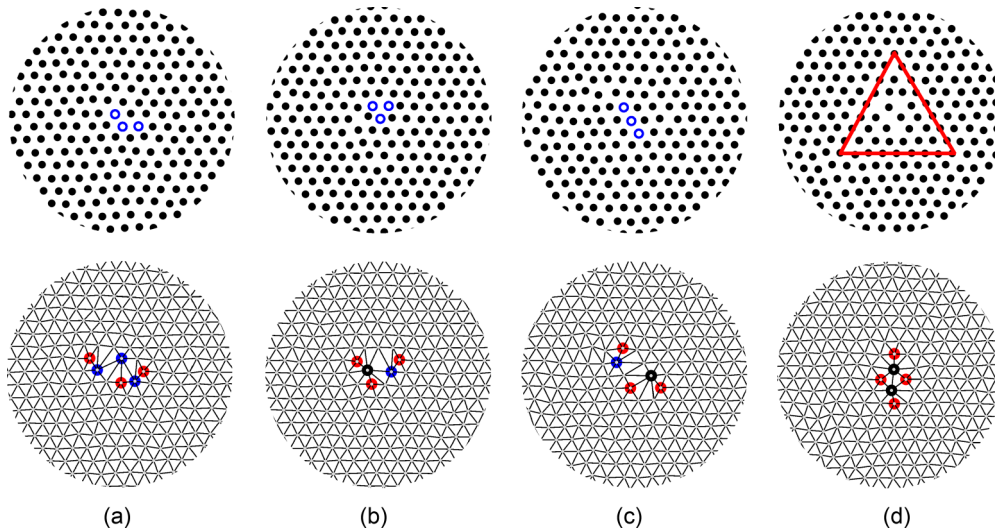

FIG. 5. (Color online) The morphologies of the originally horizontally oriented three-point vacancy found in MD simulations during the temperature range $T \in (0.1, 0.3)$. The empty blue circles in the upper row indicate the vacant sites. The lower row shows the defect structures via the Delaunay triangulation. The red, blue, and black dots represent five-, seven-, and eight-fold disclinations, respectively.
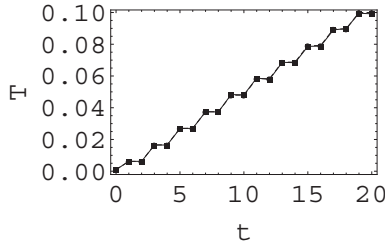
FIG. 6. The scheme to increase the temperature to identify the critical value $T_{\text{zip-up}}$ at which a linear vacancy is zipped up. The excellent overlap of the preset temperature variation (solid line with squares) and the real temperature variation (dashed line with dots) is an indicator of high-quality simulations. The time is measure in the unit of $5125\tau_0$.

We proceed to study the case of two-point vacancies. We first discuss their stability. Simulations show that, at least during the entire running time for 10 million time steps, the two-point vacancy can preserve its integrity well at temperatures below $T_{\text{split}} \approx 0.23$. The event of the split of a two-point vacancy is observed only once at $T = 0.2$ and $T = 0.22$, respectively. The resulting two one-point vacancies are then quickly recombined. The frequency of the split and recombination of the two-point vacancy increases with temperature. At $T = 0.25$, for example, the long-time separation of the vacancy is captured in simulations as shown in Fig. 3 where D_{pp} is the separation between the two split one-point vacancies. From the abscissa in Fig. 3 we read the duration of the separated state for up to 1 million time steps. The defect structures at $t = 163$, 164, and 165 are also shown in Fig. 3. The elongated ellipse-like defect cluster in the first inset in Fig. 3 is seen to be torn apart into two topologically neutral clusters accompanying the split of the two-point vacancy. The configurations of the split defect clusters keep transforming in response to the variation of their separation. The linear 5-8-5 defect in the second inset in Fig. 3 becomes

the 5-7-5-7 defect cluster shown in the last inset while the total topological charge of these dancing defect clusters always remains zero. The separation of the two-point vacancy into two one-point vacancies may be understood thermodynamically. At sufficiently high temperature $T = T_{\text{split}}$, the split of the two-point vacancy can occur when the entropic contribution to the free energy starts to dominate over the energy required to tear the defect cluster into two.

Now we discuss the dynamics of the two-point vacancy below the split temperature T_{split} where its integrity is well preserved. The mobility of the two-point vacancy originates from the movement of a surrounding particle to fill one of the two vacant sites. In Fig. 2(b) we plot the mean squared displacement of the center of the vacancy versus time for both cases of one-point (squares, dashed, green) and two-point (triangles, dotted, red) vacancies. We see that the two-point vacancy also moves diffusively in the crystal, but with a significantly larger diffusion coefficient. This phenomenon seems counterintuitive considering the larger size of the two-point vacancy than the one-point vacancy; the diffusion coefficient of real particles is inversely proportional to the particle size according to the Stokes-Einstein relation. In comparison with the one-point vacancy case, we notice that the extra vacant site in the two-point vacancy increases the probability of being occupied by a surrounding particle which is the origin of the vacancy motion. In other words, the extra vacant site in the two-point vacancy enhances its activity of motion and facilitates the diffusion. Notably, a closer examination reveals that, in addition to moving forward or backward, the two-point vacancy can also rotate via filling a vacant site with one of the two neighboring particles on the central line perpendicular to the vacancy. The rotational motion is easier due to the lower energy barrier (see Fig. 4). To quantitatively account for the faster diffusion of the two-point vacancy in comparison with that of the one-point vacancy, we estimate the probability P_{fill} that a vacant site is occupied by any of the neighboring particles during the time interval δt.
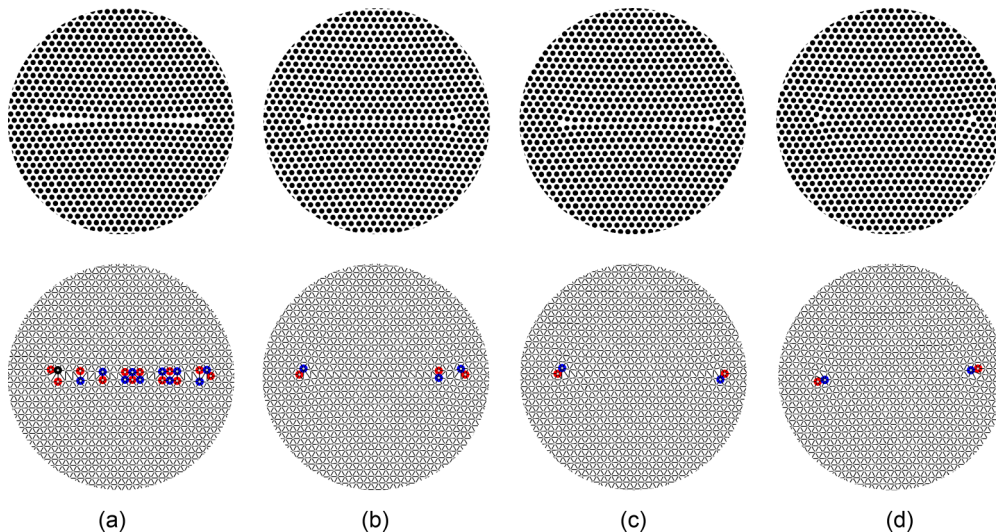

FIG. 7. (Color online) The details of the healing process of a linear vacancy with 21 missing particles revealed in MD simulations at $t = 5\tau_0$ (a), $6\tau_0$ (b), $7\tau_0$ (c), and $8\tau_0$ (d). The lower row shows the associated defect structures via the Delaunay triangulation. The red, blue, and black dots represent five-, seven-, and eight-fold disclinations, respectively. $T = 0.01$.
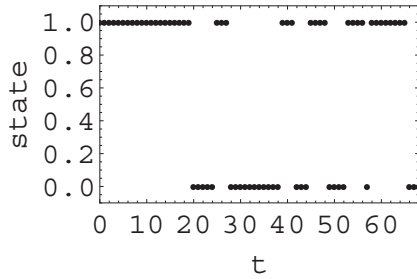
FIG. 8. The linear eight-point vacancy alternately opens and closes when the temperature is steadily increased from 0.07 (at $t = 20$) to 0.078 (at $t = 68$). The time is measure in units of $5125\tau_0$.
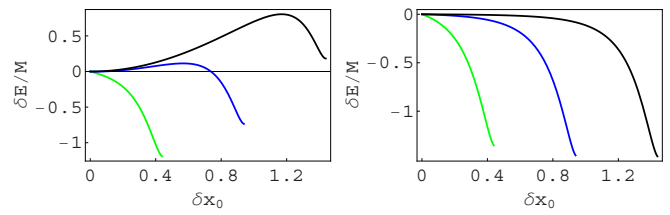

FIG. 10. (Color online) The energy variation $\delta E/M$ in the close of a linear vacancy. δx_0 is the variation of the vacancy width. The original vacancy width is $d = 2$ (lower, green), 3 (middle, blue), and 4 (upper, black), measured in the unit of the lattice spacing. The number of layers of involved particles is $n = 100$ (a), and $n = 10^6$ (b).

For the one-point vacancy case, $P_{\text{fill},1} = 6p_a$, where p_a is the probability for a neighboring particle to jump to fill the vacant site [see the inset in Fig. 4(a)]. For the two-point vacancy case, $P_{\text{fill},2} = 6p_a + 4p_b$, where p_b is the probability for the jump shown in the inset in Fig. 4(b). The factor 4 is for the four ways for the two middle particles to fill either of the two vacant sites [see Fig. 4(b)]. p_b is significantly larger than p_a for the much lower energy barrier in Fig. 4(b) than that in Fig. 4(a). To conclude, $P_{\text{fill},2} \gg P_{\text{fill},1}$, which indicates the much higher mobility of the two-point vacancy than that of the one-point vacancy.

For the three-point vacancy, the plot of $\langle r^2 \rangle$ versus time is given in Fig. 2 (dots, solid, black). Surprisingly, the mobility of the three-point vacancy is found to be reduced in comparison with the two-point vacancy. It may be attributed to the numerically observed morphological change of the three-point vacancy shown in Fig. 5. With the gradual increase of temperature from 0.1 to 0.3, the originally frozen rodlike three-point vacancy becomes deformable (during the observation time of 2 millions time steps). The observed morphologies are presented in Fig. 5, including the smeared structure (collapsed vacancies) highlighted in the red triangular box where the vacancies are "dissolved" in the crystal with a crosslike underlying defect structure. In real alkali halide crystals, these morphologies of the three-point vacancy might be distinguishable as different color centers. It is important to note that these morphological transformations do not contribute to the displacement of the three-point vacancy. The activity of motion brought by the extra vacant sites in the three-point vacancy is partially self-consumed in these morphological transformations, resulting in the reduction of the diffusion coefficient in comparison

with the two-point vacancy. Therefore, the significantly fast diffusion of the two-point vacancy provides the most efficient mechanism, among the types of the one-, two- and three-point vacancies, to realize particles migration in crystalline materials.

The further increase of the vacancy length leads to distinct dynamical scenarios. MD simulations allow us to capture the details of these events. For linear n-point vacancy of $n > 7$, simulations show that an originally open linear vacancy at sufficiently low temperature can be healed via a zip-up mechanism when the temperature increases to a critical value $T_{\text{zip-up}}$. The scheme to increase the temperature is shown in Fig. 6. A higher $T_{\text{zip-up}}$ is required to heal a shorter vacancy; $T_{\text{zip-up}}$ increases from 0.001 for $n = 11$ to 0.07 for $n = 8$. Figure 7 shows the details of the healing process of a linear vacancy at $T = 0.01$. At temperature above $T_{\text{zip-up}}$, the large positional fluctuation of particles that are exposed to the vacancy is enhanced by the van der Waals attraction which finally brings these particles together. The resulting square-lattice belt is characterized by a row of dislocations (pairs of five-fold and seven-fold disclinations) in Fig. 7(a).

This newly formed, geometrically incompatible square-lattice belt in the background of the hexagonal lattice is unstable. The instability modes can be classified into three categories depending on the length n of the vacancy. For $n = 8$, the linear vacancy alternately closes and opens in response to the increasing temperature; Fig. 8 shows the breathing mode of an eight-point vacancy when the temperature starts to increase uniformly from $t = 20$ ($T = 0.07\epsilon_0$) to $t = 68$ ($T = 0.078\epsilon_0$). For $n \in [9,15]$, the closed vacancy experiences collective
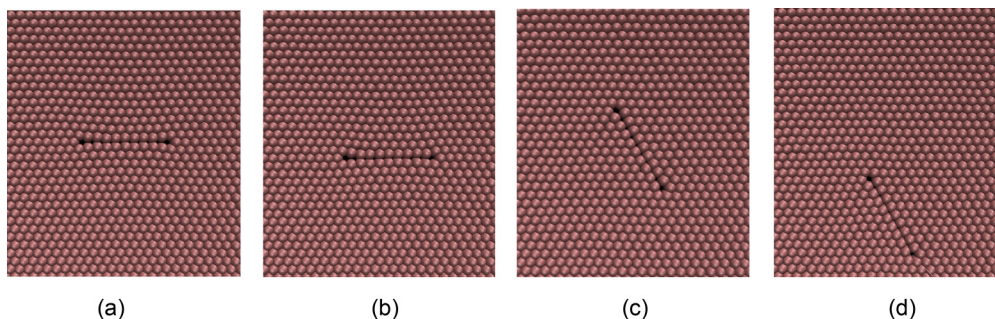

FIG. 9. (Color online) The translation and rotation of a closed linear 10-point vacancy at $T = 0.037$ (a), $T = 0.056$ (b), $T = 0.075$ (c), and $T = 0.078$ (d).

translation and rotation as a whole without destroying the belt structure (see Fig. 9). For n larger than 15, a square-lattice belt tends to be transformed to a hexagonal pattern via a translation by half of the lattice spacing [see Figs. 7(a)–7(c)]. In this transformation, the row of dislocations along the cut annihilates, leaving out a pair of dislocations that absorb all the geometric frustrations. In the process of healing a linear cut in the two-dimensional L-J crystal, we perform heuristic calculations at zero temperature and illustrate that the participation of more layers of surrounding particles can reduce the associated energy barrier and facilitate the healing process.

Consider a long linear vacancy of width d and length Mb in the middle of the two-dimensional crystal. b is the balance distance of the L-J potential $V(r)$. We calculate the energy variation when the width shrinks by $2\delta x_0$. The $n + 1$ layers of particles on each side of the linear vacancy labeling from $i = 0$ to n are subject to a displacement in the healing of the vacancy. To simplify the calculation, we only consider the interaction between neighboring particles. And the horizontal distance between neighboring particles is assumed to be invariant while the width of the layer i increases from $c = \sqrt{3}b/2$ to $c' = (ci + \delta x_0)/i$. We finally obtain the energy variation δE with the shrinking of the vacancy width by $2\delta x_0$:

$$\delta E(\delta x_0)/M = 4n[V(b') - V(b)] + 2[V(\ell') - V(\ell)] + [V(d') - V(d)],$$

where $b' = \sqrt{c'^2 + (b/2)^2}$, $\ell = \sqrt{b^2 + d^2}$, and $\ell' = \sqrt{b'^2 + (d - 2\delta x_0)^2}$. The plot of $\delta E/M$ versus the displacement δx_0 in Fig. 10 shows that the participation of more particles; i.e., larger n can reduce the energy barrier to close the vacancy and therefore facilitate the healing of the crystal.

In addition to the thermodynamics states of the L-J crystal represented by the NPT ensemble, here we also report the dependence of the one-point vacancy mobility on the particle density using the NAT ensemble; the particle density is controlled by changing the area A. Simulations show that the increase of particle density does not change the integrity of the one-point vacancy as well as the diffusive nature of the motion. In contrast, the reduction of the particle density finally leads to the emergence of holes; they start to scatter in the crystal when the particle density is below 0.82 corresponding to the lattice spacing $a = 1.18\sigma_0$. Figure 11 shows that the diffusion coefficient is rapidly reduced with the increase of the particle density. The increasing particle density in L-J crystals tends to immobilize vacancies. It can be attributed to the significant
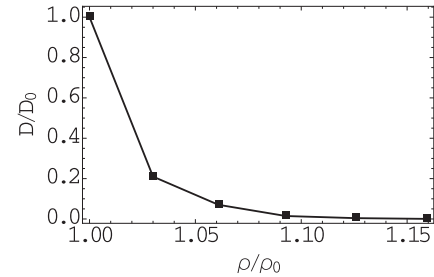

FIG. 11. The reduction of the mobility of the one-point vacancy with the increase of the particle density. D_0 is the diffusion coefficient at the particle density $\rho_0 = 0.92$ corresponding to the lattice spacing $a = r_m$. $N = 19\,999$. $T = 0.3$.

increase of the energy barrier for a vacancy to move with the reduction of the lattice spacing; the decrease of the lattice spacing by 3% and 5% will lead to the increase of the energy barrier by 46% and 94%, respectively.

IV. CONCLUSION

In summary, we study the dynamics of n-point vacancies supported by the two-dimensional Lennard-Jones crystals. The integrity and the diffusive motion of vacancies are associated with the basic feature of the local minimum in the L-J potential. Therefore, the results in this study can provide conceptual understanding of the formation and dynamics of vacancies in systems with other types of potentials who also possess sufficiently deep valley structures. In contrast, under pure repulsive potentials the vacancies were observed to be collapsed to dislocations; the diffusion of the dislocaitons were experimentally observed [13]. In our study, the healing of a linear vacancy leads to a pair of dislocations, suggesting the intimate connection between vacancies and topological defects. The interplay and mutual conversion of vacancies and topological defects constitutes an interesting theoretical problem and may provide an extra dimension in the engineering of defects in extensive crystalline materials [9].

[1] M. J. Bowick and L. Giomi, Adv. Phys. **58**, 449 (2009).

[2] E. Auyeung, T. Li, A. J. Senesi, A. L. Schmucker, B. C. Pals, M. Olvera de la Cruz, and C. A. Mirkin, Nature (London) **505**, 73 (2013).

[3] D. J. Wales, ACS Nano **8**, 1081 (2014).

[4] V. Koning and V. Vitelli, arXiv:1401.4957.

[5] A. Hashimoto, K. Suenaga, A. Gloter, K. Urita, and S. Iijima, Nature (London) **430**, 870 (2004).

[6] G. D. Lee, C. Z. Wang, E. Yoon, N.-M. Hwang, D.-Y. Kim, and K. M. Ho, Phys. Rev. Lett. **95**, 205501 (2005).

[7] J. F. Shackelford, *Introduction To Materials Science For Engineers*, 7th ed. (Prentice Hall, New Jersey, USA, 2008).

[8] D. S. Fisher, B. I. Halperin, and R. Morf, Phys. Rev. B **20**, 4692 (1979).

[9] D. R. Nelson, *Defects and Geometry in Condensed Matter Physics* (Cambridge University Press, Cambridge, 2002).

[10] G. Meng, J. Paulose, D. R. Nelson, and V. N. Manoharan, Science **343**, 634 (2014).

[11] C. Knorowski, and A. Travesset, Soft Matter **8**, 12053 (2012).

[12] M. Rossi, E. Vitali, D. Galli, and L. Reatto, J. Phys. Conf. Ser. **150**, 032090 (2009).

[13] A. Pertsinidis and X. S. Ling, Nature (London) **413**, 147 (2001).

[14] R. Mas-Balleste, C. Gomez-Navarro, J. Gomez-Herrero, and F. Zamora, Nanoscale **3**, 20 (2011).

[15] A. Pertsinidis and X. S. Ling, Phys. Rev. Lett. **87**, 098303 (2001).

[16] A. Pertsinidis and X. S. Ling, New J. Phys. **7**, 33 (2005).

[17] T. H. Zhang and X. Y. Liu, Appl. Phys. Lett. **89**, 261914 (2006).

[18] D. Frenkel and D. J. Wales, Nat. Mater. **10**, 410 (2011).

[19] T. H. Zhang and X. Y. Liu, Chem. Soc. Rev. **43**, 2324 (2014).

[20] P.-A. Geslin, G. Ciccotti, and S. Meloni, J. Chem. Phys. **138**, 144103 (2013).

[21] L. Modesto, D. Júnior, J. Teixeira Rabelo, and L. Cândido, Solid State Commun. **145**, 355 (2008).

[22] P. N. Ma, L. Pollet, M. Troyer, and F. C. Zhang, J. Low Temp. Phys. **152**, 156 (2008).

[23] W. Lechner and C. Dellago, Soft Matter **5**, 2752 (2009).

[24] B. He and Y. Chen, Solid State Commun. **159**, 60 (2013).

[25] C.-H. Chiang and L. I, Phys. Rev. Lett. **77**, 647 (1996).

[26] A. Libál, C. Reichhardt, and C. J. Olson Reichhardt, Phys. Rev. E **75**, 011403 (2007).

[27] C. Durniak and D. Samsonov, Europhys. Lett. **90**, 45002 (2010).

[28] L. DaSilva, L. Candido, G.-Q. Hai, and O. Oliveira Jr., Appl. Phys. Lett. **99**, 031904 (2011).

[29] C. Durniak, D. Samsonov, J. F. Ralph, S. Zhdanov, and G. Morfill, Phys. Rev. E **88**, 053101 (2013).

[30] W. Lechner and C. Dellago, Soft Matter **5**, 646 (2009).

[31] J. N. Israelachvili, *Intermolecular and Surface Forces,* 3rd ed. (Academic Press, New York, 2011).

[32] O. Vinogradov, Comput. Mater. Sci. **45**, 849 (2009).

[33] Z. Yao and M. Olvera de la Cruz, Phys. Rev. E **87**, 042605 (2013).

[34] Z. Yao and M. Olvera de la Cruz, Phys. Rev. Lett. **111**, 115503 (2013).

[35] M. Antlanger, M. Mazars, L. Šamaj, G. Kahl, and E. Trizac, Mol. Phys. **112**, 1336 (2014).

[36] Available at http://lammps.sandia.gov

[37] S. Plimpton, J. Comput. Phys. **117**, 1 (1995).

[38] Z. Yao and M. Olvera de la Cruz, Proc. Natl. Acad. Sci. USA **111**, 5094 (2014).

[39] M. Bowick, H. Shin, and A. Travesset, Phys. Rev. E **75**, 021404 (2007).

[40] W. T. Irvine, M. J. Bowick, and P. M. Chaikin, Nat. Mater. **11**, 948 (2012).